A High Power Liquid Hydrogen Target for Parity Violation Experiments

E.J. Beise,[3] D. H. Beck,[2] E. Candell,[4] R. Carr,[1] F. Duncan,[3] T. Forest,[2] W. Korsch,[1] J. W. Mark,[5] R. D. McKeown,[1] B. A. Mueller,[1] M. Pitt,[1] S. Wells[6]

[1] *California Institute of Technology, Pasadena, California 91125*
[2] *University of Illinois at Urbana-Champaign, Urbana, Illinois 61801*
[3] *University of Maryland, College Park, Maryland 20742*
[4] *Rensselaer Polytechnic Institute, Troy, New York 12180*
[5] *Stanford Linear Accelerator Center, Stanford, California 94309*
[6] *MIT-Bates Linear Accelerator Center, Middleton, Massachusetts, 01949*

(February 20, 1999)

Abstract

Parity-violating electron scattering measurements on hydrogen and deuterium, such as those underway at the Bates and CEBAF laboratories, require luminosities exceeding $10^{38} \text{cm}^{-2} \text{s}^{-1}$, resulting in large beam power deposition into cryogenic liquid. Such targets must be able to absorb 500 watts or more with minimal change in target density. A 40 cm long liquid hydrogen target, designed to absorb 500 watts of beam power without boiling, has been developed for the SAMPLE experiment at Bates. In recent tests with 40 μA of incident beam, no evidence was seen for density fluctuations in the target, at a sensitivity level of better than 1%. A summary of the target design and operational experience will be presented.

I. INTRODUCTION

Recently there has been considerable interest in the neutral weak interaction between electrons and hydrogen or deuterium as an indicator of strange quark contributions to the internal structure of nucleons. Experiments which measure the parity-violating asymmetry in electron scattering as a signature of the neutral weak process have been proposed or

nucl-ex/9602002 14 Feb 1996

are underway at the Bates [1], CEBAF [2], and Mainz [3] laboratories. As predicted by the Standard Model for Electroweak Interactions, a parity violating asymmetry will occur in the difference in the yield for scattering of positive or negative helicity (longitudinally polarized with respect to the beam direction) electrons from an unpolarized target. The magnitude of the asymmetry is strongly dependent on the degree to which strange quark matrix elements contribute to the neutral weak response of the nucleon [4–6]. Since both the cross sections and asymmetries are small, making a measurement in a reasonable amount of beam time (less than or on the order of 1000 hours) requires luminosities exceeding $10^{38}/cm^2/sec$. This luminosity can be achieved with modern high current polarized electron beams on cryogenic liquid targets but results in a large amount of beam power deposited in the target.

Cryogenic targets which are capable of absorbing 200 watts of beam power without boiling have been used previously at SLAC [7] and Bates [8]. The new generation of both parity violation and electromagnetic physics experiments planned for Bates and CEBAF will require targets with beam power capabilities of 500 watts or more. One example is the SAMPLE experiment [1] at the Bates Laboratory, in which the parity violating asymmetry in elastic electron scattering from hydrogen and deuterium will be used to investigate strange quark contributions to the proton's magnetic moment. For this experiment, a 40 cm long liquid hydrogen target was developed which can absorb 500 watts of beam power without boiling. It is a closed loop system in which liquid is circulated by a mechanical pump at a volume flow rate of approximately 7900 cm^3/sec. The target was constructed at the W.K. Kellogg Radiation Laboratory in 1992, installed at the Bates Laboratory in 1993, and was first used in a data taking run with a 40 μA polarized electron beam in September 1995. In this paper a summary of its design and operation is presented, as well as results to date of studies of its performance with and without incident beam.

Section II describes the target system including the target loop and cell, the refrigeration system, gas handling and computer controls. It is followed in Section III by a discussion of operating experience without beam and a set of studies designed to understand the efficiency of the circulating pump and heat exchanger. The paper concludes with a discussion of operational experience with beam on target and the resulting implications for the experimental determination of the parity-violating asymmetry to be measured in the SAMPLE experiment.

II. DESCRIPTION OF THE LIQUID HYDROGEN TARGET

A. Overview

An overview of the complete SAMPLE target system is shown in figure 1. Liquid hydrogen is circulated through a closed loop inside a vacuum chamber connected to the beam line. The circulating pump is immersed in the liquid, and controlled by an AC motor which sits in a room temperature hydrogen environment outside of the vacuum chamber. The flow is

directed through a 40 cm long target cell longitudinal to the beam. The hydrogen in the target loop is cooled by a counterflow heat exchanger connected to a refrigeration system which delivers 16 psia of cold helium gas via 6 m long vacuum-jacketed transfer lines. Delivery of the hydrogen gas is controlled through a manually operated gas panel. A PC-based control system monitors the temperatures and pressures in the target system and the status of the gas panel, and operates a feedback loop between an internal heater and the incident beam current to maintain a constant heat load on the target. The nominal operating temperature and pressure of the target loop are 20 K and 2 atm.

The target fluid is cooled by a Process Systems International[1] model 1620-S refrigeration system. Helium gas at approximately 230 psig is delivered to the refrigerator by a rotary screw (RS) compressor. Part of the gas enters a liquid nitrogen precooling circuit, and the remainder passes through the first stage of a heat exchanger. The recombined gas is then cooled through a second heat exchanger, after which point the He temperature is approximately 80 K. Charcoal adsorbers remove impurities from the gas before it enters the main heat exchanger cycles. Finally, two expansion engines expand the gas and deliver it to the target at approximately 12 K and 16 psia. The refrigerator is equipped with a 1 kW internal heater which is used in a feedback loop to maintain a return gas temperature of 20 K, thus regulating the required cooling power delivered to the target. The mass flow of the coolant is determined by monitoring the temperature rise across the 1 kW heater. In principal this cycle could be used to control the target temperature when beam is incident on the target. However, in practice, changes in beam current are too rapid for this system to respond effectively, so the target liquid temperature is controlled with a feedback loop between an internal target heater and the average beam current, as discussed above.

A schematic view of the target loop is shown in figure 2(a). It consists of a heat exchanger, a pump, the target manifold and the target cell. The target manifold is made of 6061-T6 Aluminum, as are the inner workings of the pump and the target cell. All other parts are made of Type 304 stainless steel. All joining parts are mated with conflat flanges, with the exception of one indium seal at the exit of the target manifold. When full, the target loop contains approximately 25 liters of liquid.

The heat exchanger, designed for very high hydrogen throughput (~ 1 kg/sec) but low pressure, consists of an 80 cm long, 15 cm diameter copper hose inside a stainless steel pipe of approximately the same diameter. Hydrogen flows through the center of the Cu hose, and He coolant flows in a helical path between the Cu and the steel pipe, counterflow to the hydrogen. The circulating pump is connected to an AC motor via a long shaft, with one cold and one warm bearing to keep the heat load from the motor at a minimum. The motor runs between 10 and 60 Hz, controlled by a variable frequency motor controller and monitored with a tachometer. A resistive heater made of Chromel ribbon epoxied to two fiberglass boards is in direct contact with the target fluid just below the pump, and is used in a feedback loop with electron beam current to keep the target cell at a constant temperature.

Up to 1 kW of power can be deposited in the fluid.

Enclosing the target loop is a rectangular Aluminum vacuum chamber with 2.54 cm walls. The loop is suspended from the top plate of the vacuum chamber and is aligned within the chamber while it is cold and under vacuum by the use of a sliding teflon seal. Attached to the vacuum chamber is a cylindrical scattering chamber with 3.1 mm walls and no exit windows.

The circulating target fluid flows from the pump to the heat exchanger, and is delivered into the center of the target cell via a baffle in the manifold. It then flows longitudinally, antiparallel to the beam direction along the center of the target and returns to the manifold between the baffle and the cell wall. The temperature of the target is monitored in six places within the loop with Lakeshore CGR-1-2000 carbon glass sensors: the sensors are located before and after the pump (labelled T_A and T_B, respectively), on the inlet and outlet of the target manifold (T_{MI} and T_{MO}), and in two symmetric locations in the target cell (T_L and T_R). Two fill lines, located before and after the pump, connect the target loop to the gas handling system.

Figure 2(b) shows a more detailed view of the target cell and manifold. The outer wall is a 40 cm long, 7 cm diameter closed-end tube with 0.38 mm thick walls, and the inner tube has a thickness of approximately 0.13 mm. The fluid circulates from the manifold through the center tube and returns through the annulus formed by the inner and outer cell walls. The inner cylinder is tapered to 3 cm diameter at the beam entrance point in order to keep the flow rate high, and perforations in the walls of the inner tube introduce transverse flow in order to quickly remove fluid from the path of the beam.

Changes in the target length as a function of beam position are an important consideration in the measurement of small parity-violating asymmetries. To maintain a constant target length as a function of transverse position, the exit window of the target has the same radius of curvature as the entrance window. The exit window curvature is maintained by a separate He cell which backs the target cell, and the pressure of the He cell relative to the hydrogen is maintained constant by a regulator valve on the gas panel. The target thickness introduced by the helium is negligible compared to 40 cm of liquid hydrogen.

B. Gas Handling and Controls System

The gas handling system for the SAMPLE target is based on systems used with other cryogenic targets at the SLAC and Bates Laboratories [7,8]. A detailed report of the present target system, as well as operating instructions, can be found in reference [11].

Central to the system is the valve panel providing interconnection among the target loop, hydrogen and helium source bottles, a vacuum pump and a 2500 liter ballast tank for hydrogen. Figure 3 shows an abbreviated schematic of the gas handling system. A complete

gas handling diagram can be found in [11].

Before cooling, the target is pumped, purged and then filled to its operating pressure of 30 psia, as determined by pressure gauge P3. In order to avoid damage to the helium cell, its pressure must not exceed the target pressure by more than 15 psid, so the target and helium cell are filled in two stages. In addition, as the target is cooled, the target pressure must never exceed the pressure in the helium cell by more than 1 psid. The pressure difference across the convex entrance window to the helium cell is kept at 0 psid by pneumatic relay R11, and monitored by pressure gauge P8. The target fluid is circulated while it is cooled and liquified, and the differential pressure generated by the circulating pump is monitored by pressure gauge P9. When the loop is full of liquid, the hydrogen supply is closed and the operating pressure is maintained by the large volume of hydrogen in the ballast tank, through pneumatic valve PV12. The maximum pressure in the target loop is regulated by solenoid valve SV13, which is set to open at 17 psig. For safety, two additional relief valves in parallel with SV13 are set to open at 25 and 30 psig.

The target control system consists of several devices equipped with GPIB interface electronics connected to a personal computer. This system performs several functions, the most important of which is to monitor the state of the gas handling system and the temperature and pressure of the target. Two control functions are also performed by the PC. The temperature of the target is regulated through a feedback loop between the internal target heater and the average beam current incident on the target. Movement of the target horizontally and vertically with respect to the beam direction is controlled remotely with stepping motors.

The six carbon glass temperature sensors in the target loop are monitored by a Lakeshore model 820 cryogenic thermometer. Pressure transducers, average beam current and the target internal heater current and voltage, are determined by an Iotech 8-channel ADC. The target heater current is controlled by an Iotech digital-analog converter, as are the the stepping motors used for target motion. The target position is indicated by two potentiometers whose resistances are measured by a Keithley 199 digital multimeter. Finally, the status of most of the valves on the gas panel are monitored with digital I/O registers.

III. OPERATING EXPERIENCE

In order to successfully use a cryogenic liquid target in a high current electron beam, two criteria must be satisfied. First, the overall cooling capacity of the refrigeration system must be sufficient to overcome the total power dissipated by the beam. For a 40 μA electron beam the total power deposited in 40 cm of liquid hydrogen is approximately 500 watts. Secondly, even if the total power of the beam can be absorbed, this power is not deposited uniformly, and local boiling in the path of the beam can occur. Local boiling will be manifested as fluctuations in the target density, causing non-statistical fluctuations in the experimental counting rate. The likelihood of local boiling depends on the power density of the beam,

the flow rate of the target liquid, and the geometry of the target cell. Ideally, one would measure the velocity of the fluid where the electron beam crosses the target. This is not practical in the present system for several reasons, one of which being that the flow in the target cell is designed to be highly turbulent, with a Reynold's number approaching 10^7. Our philosophy was instead to attempt to determine as much as possible about the volume flow rate of the fluid, and then to look for evidence of density fluctuations during tests with the electron beam on the target.

A. Bulk Cooling

The overall cooling capacity of the target/refrigeration system is determined by the properties of the refrigerator system and by the capabilities of the heat exchanger in the target loop. The PSI model 1620 refrigerator, described above, supplies 17 g/s of helium gas, at 16 psia and approximately 12 K, to the target loop. The supply temperature of the coolant is controlled in a feedback loop with a heater internal to the refrigerator, such that a constant (20 K) return temperature is maintained. The available power of the refrigerator is therefore approximately the set value of the refrigerator heater, and any heat load from the target will cause a drop in the refrigerator heater power. The dominant loads are the power deposited by the beam, the power on the internal target heater, and the power dissipated by the circulating pump. Radiative losses are negligible. The total available power is typically 700 watts when the LN_2 precooling circuit is used and 450 watts without LN_2 precooling.

B. Determination of the mass flow rate

The mass flow dm/dt of the circulating fluid in the closed loop can be determined from its temperature rise across a known power source. For the expected mass flow of liquid hydrogen in the SAMPLE target, a power deposition of 1 kW will cause a temperature rise of only 0.3 K. With helium gas at 20 K and 2 atm as the target fluid, a temperature difference of several degrees is expected, so initial studies of the pump were performed with helium gas. The mass flow and the power deposition by the target heater, Q_H, are related by

$$\frac{dQ_H}{dT} = c_V \frac{dm}{dt} \tag{1}$$

where c_V is the specific heat at constant volume of the fluid. Here we use c_V and not c_P because the measurements are performed with a fixed volume of gas. The pump efficiency, ε, is determined from the mass flow through

$$\frac{dm}{dt} = V_s \varepsilon f \rho \tag{2}$$

where V_s is the geometrical pump displacement (~ 550 cm^3/cycle), f is the frequency of the motor (Hz), and ρ is the density of the fluid. For LH$_2$ at the design parameters passing through a 100% efficient pump operating at 60 Hz, the mass flow would be 2300 g/s (as outlined below, the flow rate used during the experiment was four times lower). The equivalent mass flow for cold helium gas (2 atm, 20 K) is 100 g/s. In order to meet the design requirement of a linear velocity of 10 m/s in the target cell, a pump efficiency of 0.5 or better is required at f=60 Hz (assuming completely longitudinal flow in the target cell).

Temperature difference measurements in helium were performed at pump speeds of 20, 30 and 60 Hz. The heater inlet temperature was taken to be the average of three sensors (see figure 2), T_L, T_R and T_{MI}; the sensor directly below the heater was not functioning. The outlet temperature was taken to be the sensor directly above the heater, T_A. Figure 4(a) shows the temperature differences vs. heater power, each fitted to a straight line. In figure 4(b) is shown the calculated mass flow from the fits, compared to that expected for a 100% efficient pump.

Similar measurements were performed with LH$_2$, at pump speeds of 20, 30 and 40 Hz. In this case, only sensors T_A and T_{MI} were used to calculate the temperature difference across the heater. In order to extract mass flow rates from these measurements it was necessary to account for the temperature dependence of the specific heat and to a lesser degree, the density of liquid hydrogen. Figure 5(a) shows the temperature differences, corrected for density and specific heat variations, for the three data sets, each fitted to a straight line, and figure 5(b) shows the calculated mass flow vs. pump speed. The errors in the mass flow determination were estimated to be about 10%: the dominant error is the absolute uncertainty in the fluid temperature, resulting in an uncertainty in the specific heat. The pump efficiency is clearly lower for the 30-times denser liquid than for 20 K helium gas. The data also might indicate that the pump efficiency is dropping as the mass flow increases, which could mean that the pump is reaching a mass flow limit. Additional data at higher mass flows would be desirable. Assuming no mass flow dependence, the average of the three values is 45%, and the dotted line is the calculated mass flow using this value.

C. Pump speed studies

Studies of the pressure difference across the pump and of the available refrigerator power were performed as a function of pump speed. The dominant load on the circulating pump is expected to be the mechanical power required to reverse the direction of the liquid in the target cell. This represents a heat load on the refrigerator, and if the pump efficiency is independent of the total mass flow it can be shown [10] that the heat load should be proportional to the cube of the fluid velocity in the target cell, and therefore to the cube of the pump speed.

Figure 6(a) shows the available refrigerator power vs. pump speed f for measurements with helium gas, compared to a fit to f^3. In figure 6(b) is the equivalent information for

two different data sets of LH_2 taken in August 1993 and May 1995. The ratio of the power loads should equal the ratio of the product of the fluid densities and pump efficiency cubed. A comparison of the results for He gas and hydrogen liquid confirms the reduced pump efficiency for hydrogen fluid seen in the temperature difference measurements.

Related to the mechanical power dissipated in the target is the pressure difference across the circulating pump. The pressure head of the pump is the power required to reverse the flow of the liquid divided by the volume flow rate through the pump. It should be proportional to f^2, as long as the pump efficiency does not depend on the pump speed. In figure 6(c) is shown the measured pressure difference across the pump vs. f for LH_2, compared to a quadratic fit. In the case of helium gas, the pressure head is too small (~ 0.02 psid) to be reliably determined with the existing instrumentation.

The very good fit of $P \propto f^3$ and $\Delta p \propto f^2$ for the LH_2 data implies no mass flow dependence to the pump efficiency, in contrast to the temperature difference measurements. Future investigations with liquid deuterium will help clarify this point because of the factor of two greater mass flow of LD_2 compared to LH_2.

D. Extraction of the heat exchange coefficient

Another useful piece of information is the overall heat transfer coefficient of the target heat exchanger. The heat transfer in a simple counterflow heat exchanger is [9]

$$Q_T = U A_0 \Delta T_{LM} \tag{3}$$

where U is the overall heat exchange coefficient, and A_0 is the effective surface area of the heat exchanger (for the SAMPLE target $A_0 = 5322$ cm^2). The *log mean temperature difference* $\Delta T_{LM} = (\Delta T_o - \Delta T_i)/ln(\Delta T_o/\Delta T_i)$ where ΔT_i and ΔT_o are the differences between the coolant and the target fluid temperatures at the inlet and outlet, respectively, to the heat exchanger. U has three parts, h_1 coming from the coolant, h_0 coming from the copper walls, and h_2 coming from the target fluid:

$$\frac{1}{U} = \frac{1}{h_1} + \frac{1}{h_0} + \frac{1}{h_2} . \tag{4}$$

The thermal conductivity of the wall is very high and h_0^{-1} is negligible. For the coolant and target gases, h_i is determined from the thermodynamic properties of the fluid and its mass flow. The coolant gas coefficient is regulated by the refrigerator at $h_1^{-1} = 22$ cm^2-K/W, as determined by measured temperature differences across the refrigerator heater. For the target fluid, $h_2 \propto (\rho f \varepsilon)^{0.8}$. With LH_2 in the target, U is almost entirely determined by h_1 and is not very sensitive to the LH_2 mass flow. With helium gas as the target fluid U is strongly dependent on the target mass flow. Figure 7(a) shows typical values of ΔT_{LM} vs. target heater power for helium gas in the target loop, at three different pump speeds.

8

The lines in figure 7(b) are calculated values of U for helium, LH_2 and LD_2, compared to h_1^{-1} for the coolant only. It is possible to estimate h_2 from measured values of ΔT_{LM} as a function of target heater power. The resulting determinations of U are plotted as data points on figure 7, assuming pump efficiencies of 100% for helium gas and 45% for hydrogen liquid. The measured heat exchange coefficients are in good agreement with the calculations. (The somewhat higher value of U measured for hydrogen is a result of higher mass flow of the coolant gas for that particular data point compared to what was used in the calculation.)

In summary, several different methods indicate a pump efficiency of about 45% for LH_2, corresponding to a mass flow of about 550 g/s at 30 Hz. As indicated by the refrigerator power curves in figure 6(b), running the pump at speeds greater than 30 Hz puts too large a load on the refrigerator to adequately dissipate the bulk power deposited by the 40 μA electron beam. Pump operation is therefore limited to about 30 Hz. The resulting flow velocity in the target cell would be 5 m/s if the flow were purely longitudinal.

In order to relate this result to implications for a given experiment, one can make a rough estimate of the temperature rise in the target from beam heating by assuming that the highly turbulent fluid has a small transverse component. For example, one can determine how long a packet of fluid will remain in the beam if the average direction of travel is at 10° with respect to longitudinal. For a beam spot 3 mm in diameter, a packet of fluid will remain in the beam for about 1.7 msec or a little more than one beam pulse. During that time the temperature of the fluid in the 40μA beam will rise about 0.5 K, but will then be rapidly mixed with the surrounding fluid. As long as the fluid is kept about 2 K below the boiling point it will not boil. With completely longitudinal flow the situation is very different: the fluid spends about 80 msec in the beam and would reach its boiling point in about 10 msec. The temperature rise of the target fluid is thus strongly dependent on knowledge of the flow pattern of the fluid. It would therefore be useful to have an independent experimental signature of density variations as a function of average incident beam current.

E. Operational experience with beam on target

With a pulsed electron beam it is possible to vary the average power deposition in the target by keeping the peak current of the beam constant and changing the number of incident pulses per second. This is convenient for an experiment such as SAMPLE where the detector signal is integrated over a single beam pulse. As configured for SAMPLE, the Bates electron beam has a pulse width of 15 μsec, a maximum peak current of 5 mA and a maximum repetition rate of 600 Hz, corresponding to a maximum duty cycle of 0.9%. The beam current is varied from 0-40 μA by changing the repetition rate. Elastically scattered electrons are detected in the backward direction by collecting Cerenkov light in ten sets of mirrors and photomultiplier tubes. Because the target is unpolarized, the difference in the detector yield (normalized to incident beam charge) for right- and left-helicity incident electrons should be due to parity violation in the electron scattering process. The counting rate in each photomultiplier tube is very high, therefore individually scattered electrons are

not detected, but the signal in the photomultiplier tube is integrated over the 15 μsec beam pulse and normalized to the incident beam charge in each pulse.

Background processes and fluctuations in the electron beam cause the counting rate in the SAMPLE detector to vary by 2-3% over the course of a ten-minute run. The average counting rate normalized to incident beam charge is therefore not sufficiently stable to unambiguously identify very small changes in target length. What is more stable against fluctuations in the beam is the pulse-to-pulse asymmetry in the detector yield between right- and left-helicity electrons.

The beam control and data acquisition systems for the SAMPLE experiment are based upon a previous parity violation experiment [12]. The helicity of the electron beam is chosen randomly, except that pairs of pulses 1/60 sec apart have opposite helicity. "Pulse-pair" asymmetries in the normalized detector signal are formed every 1/30 sec, greatly reducing sensitivity to 60 Hz electronic noise and to fluctuations in beam properties such as current, energy and position on target, which generally occur on time scales much longer that 1/30 sec. One complete set of measurements represents ten calculated asymmetries (in each of the ten "time-slots" of the 600 Hz beam) for each of the ten mirror signals. A representative histogram showing the distribution of measured asymmetries is shown in figure 8. Each entry is an average of the ten mirror asymmetries in one time slot. The measured asymmetry is a Gaussian distribution with a width Σ which is predominantly determined by the counting statistics of the detector yield per beam pulse. The average counting rate with a 40 μA beam is about 4000 electrons per pulse corresponding $\Sigma \sim 0.5\%$. If the density of the target is reduced or fluctuates at high average beam current (for constant peak current) because of target boiling, the width of this distribution should increase. By looking for systematic deviations in this width as a function of beam current it is possible to place a limit on the change in density caused by beam heating.

Measurements performed in two separate runs are shown in figures 9 (a) and (b). The first data set (a) was in Dec 1994 with an unpolarized beam of 5 mA peak current and pulse width of 13 μsec. The repetition rate of the pulses varied from 60 to 600 Hz, resulting in an average current incident on the target between 4 and 40 μA. The latter measurement (b) was in Sept 1995 with a 4 mA polarized beam and slightly wider beam pulse, resulting also in a maximum average current of 40 μA. In each case the asymmetry distribution was fitted to a Gaussian. Each data point is the fitted width Σ of the distribution with an error bar representing the error in the fit. In the Dec 1994 data, variations in beam position of about 2 mm coupled with position dependent changes in background in the detector made it necessary to correct the normalized yield as a function of beam position on target. In particular, the fluctuations in the background yield (about 25% of the total detector signal), increased by 50% for highest three repetition rates. In Sept 1995 the background in the detector was lower and the beam position was more stable so no such corrections were required, although a cut on vertical beam position was applied. As shown in figure 9(c), no change in the normalized detector yield was seen as a function of beam current at the level of 1%. In the Dec 1994 data, the solid line indicates the average value of Σ for the first 5 data points, and the dashed lines are three standard deviations from the mean value.

Deviations in the width were determined from this baseline. Since the September 1995 data set consists of only four measurements, the 120 Hz datum was taken as the baseline.

The experimental asymmetry is determined by

$$A = \frac{N_+ - N_-}{N_+ + N_-} , \tag{5}$$

where N_+ (N_-) is the detector signal normalized to incident beam charge for right- (left-) handed electrons. The statistical error in the determination of A for each pulse-pair is determined by fluctuations in the incident beam charge I, the target length t, and in the number of photoelectrons collected in the photomultiplier tube N_{pe}:

$$\Sigma^2 = (\frac{\Delta A}{A})^2 = (\frac{2\Delta I}{I})^2 + (\frac{\Delta t}{t})^2 + (\frac{\Delta N_{pe}}{N_{pe}})^2 \tag{6}$$

It is possible to place a limit on target length variation by attributing all of the variation in the measured Σ to $\frac{\Delta t}{t}$. With this assumption, the observed change in Σ at 600 Hz in the Dec 1994 data would correspond to a change in target length of 0.1%. The temperature dependence of the liquid density alone would result in a change in Σ of this magnitude. Clearly no significant density change indicative of a phase transition is seen.
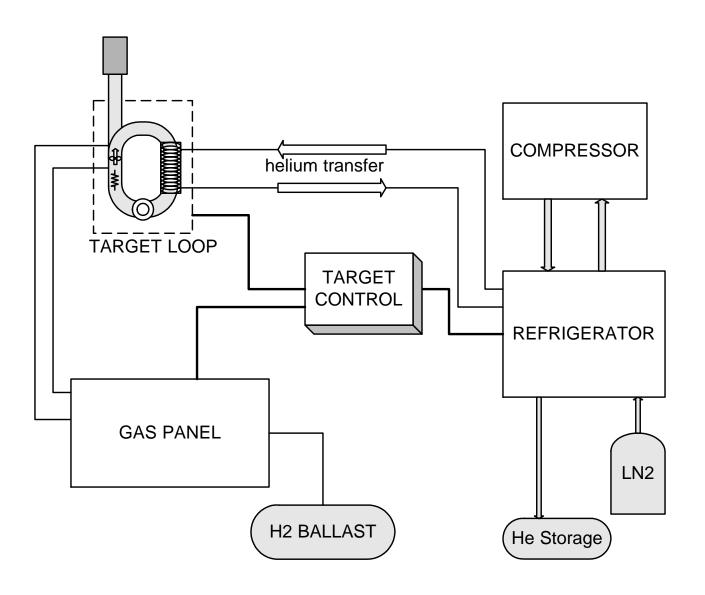
IV. CONCLUSIONS

Upcoming experiments at Bates and CEBAF require the use of cryogenic hydrogen and deuterium targets in the presence of high intensity electron beams corresponding to large power deposition in the target fluid. New measurements of parity violation in Møller scattering [13] in hydrogen have been proposed, which require small systematic errors and thus very small fluctuations in target density. So far, up to 40 μA of beam has been successfully used with the 40 cm SAMPLE liquid hydrogen target, corresponding to a deposited power of 500 W and a power density of 7 kW/cm^2. Asymmetry data indicate that the density fluctuations are small compared to 1%, resulting in a negligible contribution to the counting statistics of the SAMPLE experiment. This result has promising implications for the CEBAF program where as much as 100 μA is expected to be delivered to experiments in Halls A and C.
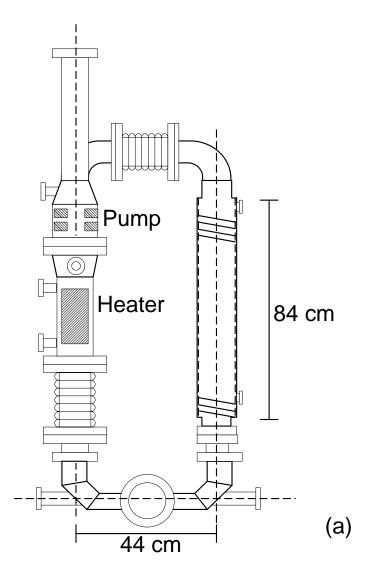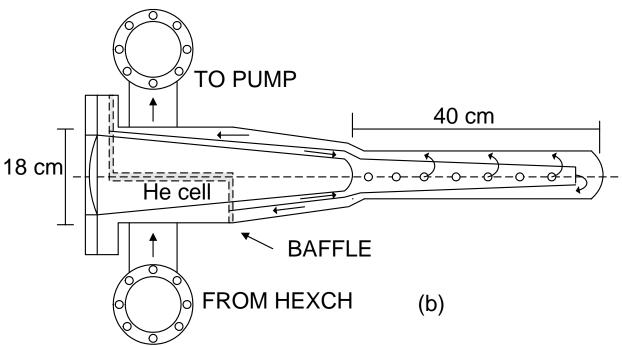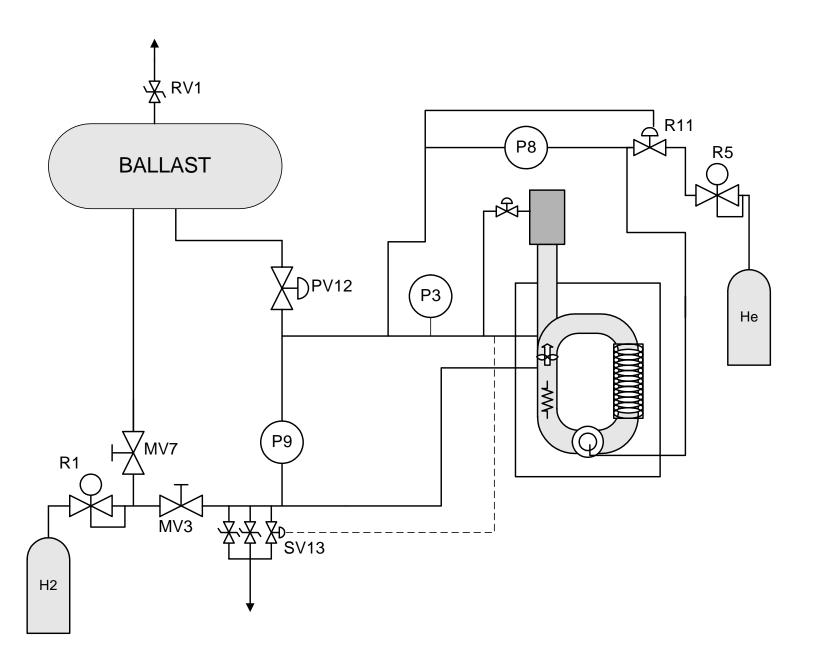
REFERENCES

[1] Bates experiments # 89-06 (D. Beck and R. McKeown) and # 94-11 (E. Beise and M. Pitt).

[2] CEBAF experiments # 91-017 (D. Beck), # 91-007 (P. Souder) and # 91-004 (E. Beise).

[3] Mainz proposal # A4/1-93 (D. von Harrach).

[4] D. Kaplan and A. Manohar, Nucl. Phys. **B310**, 527 (1988).

[5] R.D. McKeown, Phys. Lett. **B219**, 140 (1989).

[6] D.H. Beck, Phys. Rev. **D39**, 3248 (1989).

[7] J. Mark, SLAC-PUB-3169 (1983).

[8] C.F. Williamson, Bates Internal Report 88–01.

[9] see for example, *Heat Transfer*, by J.P. Holman, McGraw Hill, Inc., 1986.

[10] see for example, *Elementary Fluid Mechanics*, 7th edition, by Street, Waters and Vennard, John Wiley and Sons, 1996.

[11] E. Beise, R. Carr and E. Candell, Bates Internal Report 95–01.

[12] P.A. Souder, *et al.,* Phys. Rev. Lett. **65**, 694 (1990).

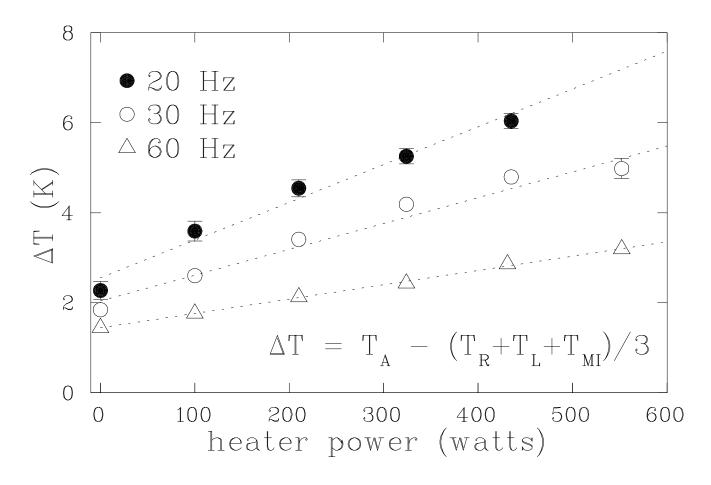[13] K. Kumar, E. Hughes, R. Holmes and P. Souder, preprint, 1996.

FIG. 1. Overall layout of the SAMPLE liquid hydrogen target system.

FIG. 2. (a) Schematic view of the target loop. (b) Schematic view of the target cell.

FIG. 3. Abbreviated layout of target gas handling system. The complete gas handling schematic can be found in the full target documentation.

FIG. 4. Temperature difference across the target heater for helium gas and three pump speeds.

FIG. 5. (a) Temperature difference, corrected for the temperature dependence of the specific heat and density of hydrogen, across the target heater as a function of heater power for three pump speeds. (b) Mass flow calculated from (a), compared to that expected for a pump efficiency of 45%.

FIG. 6. Available refrigerator power as a function of pump speed for (a) helium gas and (b) liquid hydrogen. (c) Pressure head vs. pump speed for liquid hydrogen.

FIG. 7. (a): Log mean temperature difference across the heat exchanger with helium gas as target fluid. The lines are to guide the eye only. (b) Overall heat exchange coefficient for different target fluids, compared to the heat exchange coefficient of the coolant gas alone. The lines represent calculated performance using a pump efficiency of 100% for helium gas and 45% for the liquids. The points are values extracted from measured average target temperature as a function of target heater power.

FIG. 8. Typical distribution of measured asymmetries in a half-hour run. Each entry represents an average of the asymmetry calculated for each of the ten mirror signals.

FIG. 9. Width of pulse pair asymmetry as a function of average beam current. The data in (a) are with 5 mA peak current of unpolarized beam (Dec. 1994), and in (b) are with 4 mA peak current of polarized beam (Sept. 1995). Panel (c) shows the total normalized detector signal vs. beam current for data set (b). The dashed line is the mean value and the dotted lines are 3σ deviation from the mean.

TARGET LOOP

helium transfer

COMPRESSOR

TARGET
CONTROL

REFRIGERATOR

GAS PANEL

H2 BALLAST

LN2

He Storage

Pump

Heater

84 cm

44 cm

(a)

TO PUMP

40 cm

18 cm

He cell

BAFFLE

FROM HEXCH

(b)

RV1

BALLAST

P8

R11

R5

He

PV12

P3

MV7

R1

P9

MV3

SV13

H2

$$\Delta T = T_A - (T_R + T_L + T_{MI})/3$$

line: $\epsilon = 100\%$

Top panel:

^{4}He gas

(target heater = 208 W)

$Q_F = A + Bf^3$

A = 576 W

B = -0.38×10^{-3} W$-$s^3

Q$_F$ (watts) vs pump speed (Hz)

Middle panel:

LH$_2$

$Q_F = A + Bf^3$

● Aug 93:

A = 724 W

B = -2.37×10^{-3} W$-$s^3

○ May 95:

A = 763 W

B = -1.92×10^{-3} W$-$s^3

Q$_F$ (watts) vs pump speed (Hz)

Bottom panel:

$\Delta P = A + Bf^2$

A = $\quad$ -0.02 psid

B = $\quad$ 3.33 Pa$-$s^2

LH$_2$

P9 (kPa) vs pump speed (Hz)

Top panel: $\Sigma_0 = 0.335 \pm 0.002$, Amirtot Σ (%), December 1994

Middle panel: $\Sigma_0 = 0.408 \pm 0.003$, Amirtot Σ (%), September 1995

Bottom panel: Normalized Yield (pe/nC)

Repetition Rate (Hz)